



Ground Motion Prediction Equation Applicable to Mega Earthquakes Considering Strong-Motion Generation Areas

S. Ohno ⁽¹⁾

⁽¹⁾ Associate Professor, IRIDeS, Tohoku University, Japan, ohnos@archi.tohoku.ac.jp

Abstract

Ground motion prediction equations (GMPEs) are essential to evaluate seismic hazard, seismic risk, and also earthquake insurance. Recently, earthquake records around M9 have been observed such as the 2010 Maule, Chile earthquake (Mw8.8) and the 2011 Tohoku, Japan earthquake (Mw9.0). For estimating such mega earthquakes by GMPEs, the functional forms become more important because such strong-motion records are rarely obtained.

A ground motion prediction equation for strong motion spectra is empirically developed using the 1996-2015 K-NET and KiK-net database in Japan. The Mw and distance range from 4.5 to 9.0, and less than 300km, respectively. The GMPE parameters are Mw, stress drop, Xeq, region of Q, Vs30 and basin depth. As Xeq can incorporate the effects of fault extension and inhomogeneous energy radiation, and stress drops with Mw can incorporate short-period acceleration level into GMPE, the developed GMPE is applicable even for mega earthquakes with several SMGAs. Site amplification factors are also modeled by Vs30 and basin depth. Nonlinear site amplification correction factor is also investigated.

Keywords: Ground Motion Prediction Equation, Mega Earthquake, Strong motion Generation Area



1. Introduction

Ground motion prediction equations (GMPEs) are essential to evaluate seismic hazard, seismic risk, and earthquake insurance, *etc.* Although it is difficult to take into account effects of complex phenomena such as detailed faulting process or basin-induced surface waves, the method is widely used because of its stability and easiness to apply. Recently, earthquake records around M9 have been observed such as the 2010 Maule, Chile earthquake (Mw8.8) and the 2011 Tohoku, Japan earthquake (Mw9.0). For estimating such mega earthquakes by GMPEs, the functional forms become more important because such strong-motion records are rarely obtained.

In this paper, a new GMPE, which is applicable to mega earthquake with strong-motion generation areas (SMGAs), is developed by adopting X_{eq} and stress drop (equivalent to short-period acceleration level), based on the recent Japanese strong motion records including the M9 earthquake.

2. Data

Datasets used in this paper is the NIED K-NET and KiK-net strong-motion data in Japan, selected under the conditions that the JMA magnitudes are more than 5.0, the hypocentral distances are less than 300km, and F-net or Global CMT solutions are available. The period of the datasets is from the start of the observation (1996 for K-NET and 1998 for KiK-net) and up to the year-end of 2015. Based on the hypocenter location, the earthquakes are categorized into three types: shallow inland (IL), subduction of the Pacific plate (PAC), and subduction of the Philippine Sea plate (PHI) earthquakes. Note that the subduction earthquakes include intra-slab earthquakes.

Figure 1 shows the relationships between moment-magnitude (M_w) and focal depth (CMT solution depth by F-net or Global CMT), the relationships between M_w and equivalent hypocentral distance X_{eq} [1] of the datasets for each earthquake type, the number of records, and the relationship between V_{s30} (averaged S-wave velocity from the ground surface to 30m depth) and D_{20} (the upper depth of the layer whose S-wave velocity of 2.0km/s).

The number of earthquakes is 214, 795, and 95 for IL, PAC, and PHI, respectively. The number of stations are 1145, 696 for K-NET and KiK-net, respectively. The number of records are 231,492, depending on frequency as shown in Fig. 1 due to the existence of low frequency noises. The magnitudes range from 4.5 to 9.0 (the 2011 Tohoku earthquake) for PAC, while up to 6.9 for IL and up to 7.4 for PHI. The centroid depths are up to 240km, while many of them are less than 70km. The epicenter and station locations are shown in Figs. 3 and 5, respectively.

As a source-to-site distance, X_{eq} is used to take into account the effect of fault extension and inhomogeneous energy radiation. For major earthquakes in the datasets (mostly, $M_w > 7$ for PAC, $M_w > 6.5$ for PHI and IL), X_{eq} is calculated by Eqs. (1) and (2),

$$X_{eq}^{-2} = \frac{\sum_i (A_i^2 X_i^{-2})}{\sum_i A_i^2} \quad (1)$$

$$A_i \propto M_{oi}^{1/3} \Delta\sigma_i^{2/3} \quad (2)$$

where X_i is distance between the site and i -th subfault, A_i , M_{oi} and $\Delta\sigma_i$ are short-period level, seismic moment and effective stress (stress drop) of the i -th subfault, respectively. Eq. (2) is derived from omega-squared model of source spectrum. When SMGA model is not available, slip is used as A_i instead. By using EHD, the extended fault can be treated as point source for each pair of fault and station [1]. Hypocentral distance is used as X_{eq} for the smaller earthquakes.

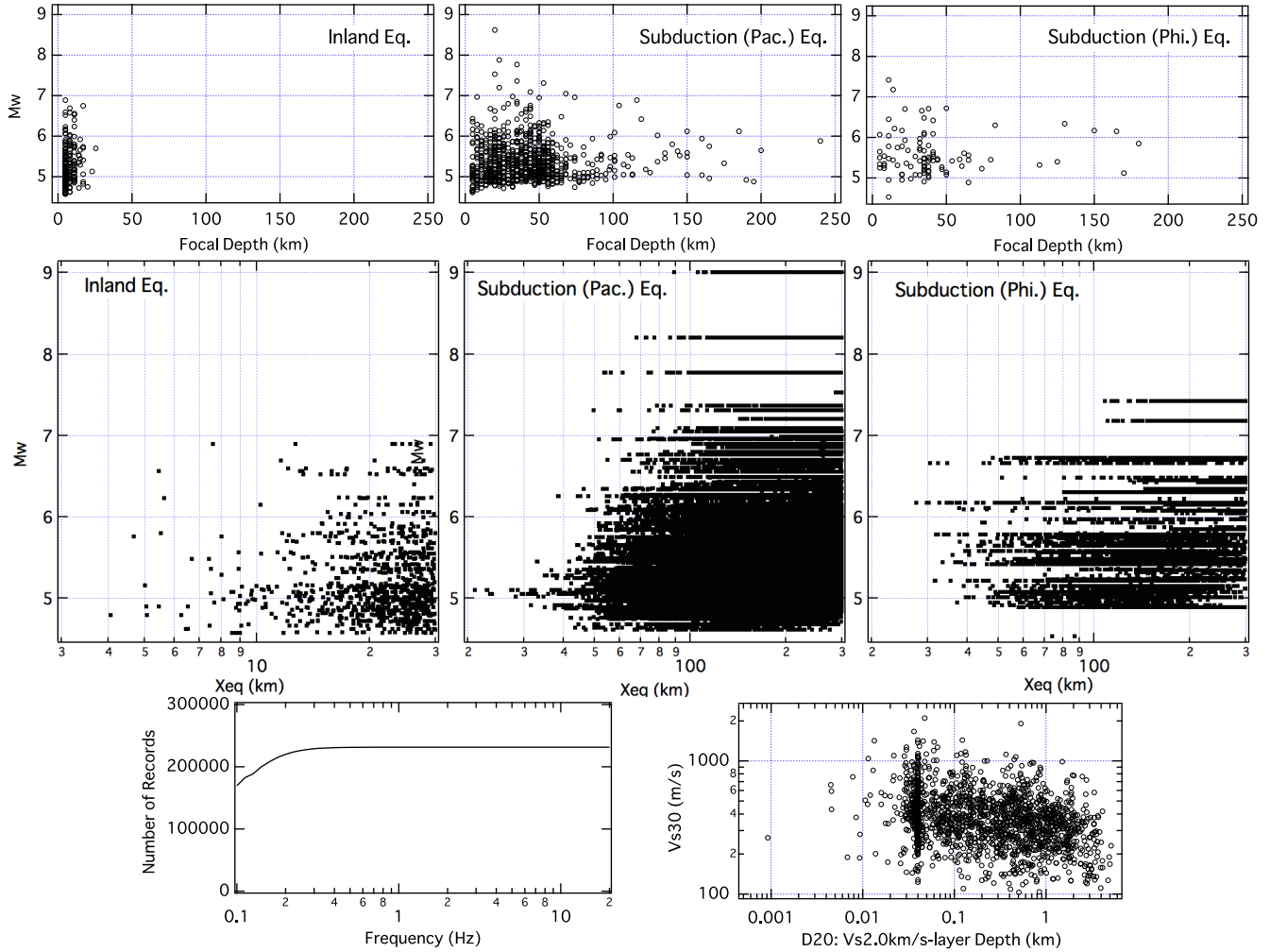


Fig. 1 –Distribution of the Data. Mw-distance (top), Mw-Xeq (middle), number of records and Vs30-D20 (bottom).

3. Inversion analyses of Fourier and response spectra

At first, spectral inversion analyses are conducted for Fourier and response spectra including PGA and PGV. The formulation and estimation procedures are based on Ohno [2], while some new parameters are added. Eqs. (3) to (5) give the functional forms used for the inversion analysis.

$$O_{ij}(f) = S_i(f) \cdot P_1 \cdot \exp\left[-\frac{\pi \cdot P_2 \cdot f}{Q(f) \cdot V_s}\right] \cdot G_j(f) \quad (3)$$

$$P_1 = \begin{cases} 100^{-1} & (X_{eqij} \geq 100km, inland eq.) \\ X_{eqij}^{-1} & (otherwise) \end{cases} \quad (4)$$



$$P_2 = \begin{cases} X_{eqij} & (\text{inland eq.}) \\ X_{eqij} \frac{\Delta E}{\Delta E + \Delta W} & (\text{forarc side, subduction eq.}) \\ X_{eqij} \frac{\Delta W}{\Delta E + \Delta W} & (\text{backarc side, subduction eq.}) \end{cases} \quad (5)$$

where f is frequency, subscripts i, j indicate an earthquake and a site, respectively. O_{ij} is either Fourier spectrum FS (cm/s) of S-wave portion, 5%-damped pseudo velocity response spectrum pSv (cm/s), or PGA (cm/s²), PGV (cm/s) of total duration of the record. P_1 is the geometrical spreading factor and is modeled to express the attenuation rate change due to SmS or Lg waves for shallow inland earthquakes. $S(f)$, $Q(f)$, $G(f)$ are regression coefficients and represent earthquake terms, quality factors of the propagation paths, and site amplification factors, respectively.

P_2 is equivalent hypocentral distance and is divided into fore-arc and back-arc portions to represent different attenuation characteristics of the two regions for subduction earthquakes [3]. ΔE (km) and ΔW (km) are the fore-arc and back-arc portions of epicentral distance, divided at the volcanic front lines in Fig. 4. The geographical area where this dividing procedure applied is almost the same as Morikawa and Fujiwara [4]. Vector sum of two horizontal components is used for Fourier spectrum and geometrical mean is used for the others.

Using S-wave arrival time by the JMA travel time table 2001, and time length T_L (s) of Eq. (7) as S-wave duration, S-wave portion of each record is extracted for Fourier spectrum calculation. Considering uncertainty due to rupture direction, Eq. (7) is composed of 2.5s (minimum length of time window) and twice of rupture duration T_w in Eq. (6). T_w is obtained from dividing rupture length L (km), a function of magnitude M [5], by assumed rupture velocity V_r of 3.0 km/s.

$$T_w = L/V_r = 10^{(0.5M-1.88)}/3.0 \approx 10^{0.5M-2.4} \quad (6)$$

$$T_L = 2.5 + 2T_w \quad (7)$$

Twenty-five sites (one K-NET (IWT009) and 24 KiK-net sites) are selected as the reference sites, where 'optimized' subsurface structure models down to the seismic bedrock are available [6][7]. The observed records at the ground surface of these sites are converted to bedrock-outcropped motions using 1-D S-wave propagation theory. The amplification factors at these converted sites are assumed as two, independent of frequency. Also, to avoid the effects of nonlinear soil amplifications, the records of $PGA < 200$ (cm/s²) are used at the ground surface stations, while all records are used at the KiK-net borehole stations. The extraordinary large PGA records, where the rocking motions of the seismometer basement might be excited [8], are also eliminated. After taking logarithm (base 10) of Eq. (3), least-squares method is applied to estimate the coefficients.

3.1 Quality Factors

Fig.2 shows the Q-values calculated by Vs of 3.4 km/s for IL, 4.0 km/s for PAC and PHI, respectively. The estimated coefficients for FS show that the quality factors of the back-arc regions are smaller than fore-arc regions. In addition, Q of the PAC fore-arc region is the largest (low attenuation). The Q-values estimated from FS and pSv almost agree in the high frequency range, while the differences become larger at low frequencies. This is probably due to the effect of surface waves, because coda part is included for calculating pSv, but not included for FS as described above.

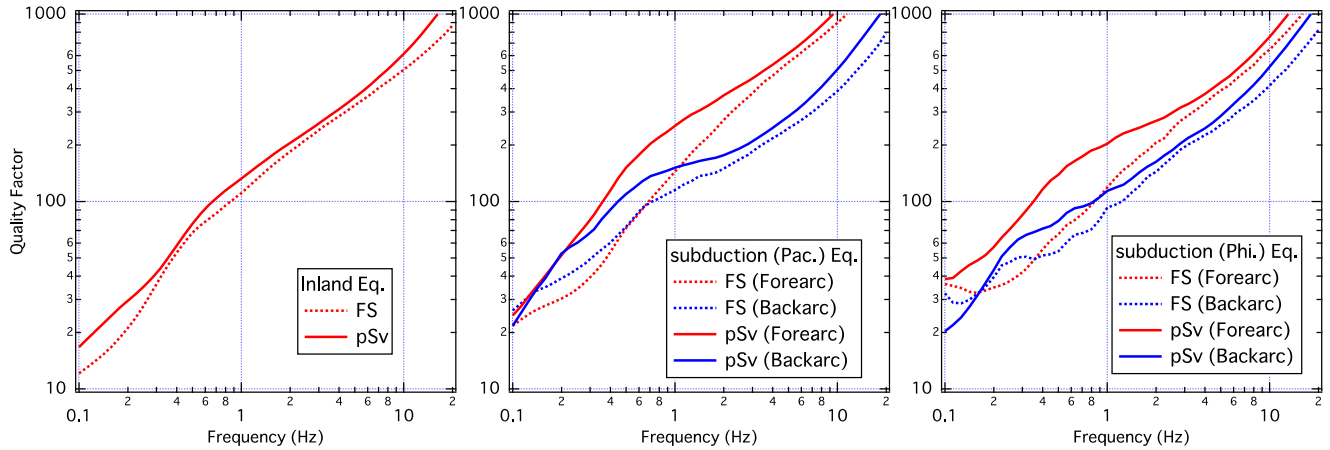


Fig. 2 – Estimated quality factors.

3.2 Stress Drop (Stress Parameter)

Source spectrum $M_{oi}(f)$ is calculated by Eq. (8) from the estimates of $S_i(f)$, under the condition that $R_{\theta\phi} = 0.63$, $\rho = 2.7 \text{ t/m}^3$ and 3.0 t/m^3 for inland and subduction earthquakes, respectively. By fitting omega-square model of Eq. (9) to $M_{oi}(f)$, only corner frequency f_c (Hz) is estimated using least-squares method because M_o is fixed from F-net or Global CMT solutions. Finally, Brune's stress drop $\Delta\sigma$ (MPa) is calculated from Eq. (10).

$$M_{oi}(f) = (4\pi\rho V_s^3 / R_{\theta\phi}) S_i(f) \quad (8)$$

$$M_{oi}(f) = (2\pi f)^2 M_o / \{1 + (f/f_c)^2\} \quad (9)$$

$$\Delta\sigma = M_o f_c / (10 \cdot (4.9 \times 10^6 V_s)^3) \quad (10)$$

Spatial distributions of the estimated stress drops are shown in Fig. 3. It is found that 1) the stress drops of subduction-zone earthquakes are larger than those of inland earthquakes, 2) deep subduction (intraslab) earthquakes along volcanic fronts or back-arc sides tend to have larger $\Delta\sigma$ than the shallower earthquakes, 3) the stress drops of inland earthquakes occurred near volcanoes in the east part of Japan have lower values than the other areas. Fig. 4 shows relationships between the estimated stress drops and the moment magnitudes and the centroid depths. The stress drops are widely scattered in the small magnitude and relatively shallow depth range, probably because of the variation of stress-state of the small faulting area. It is found that the stress drops of deep earthquakes are averagely larger than the shallow earthquakes, as pointed above.

A stress drop of 21MPa is estimated for the 2011 Tohoku earthquake (Mw9.0) and the corresponding short-period level is $3.9 \cdot 10^{20} \text{ (N}\cdot\text{m/s}^2)$. Note that this value is roughly within the range of estimates by SMGA modeling using semi-empirical waveform synthesis method: $2.1 \cdot 10^{20} \text{ (N}\cdot\text{m/s}^2)$ by Asano and Iwata [9] and $3.9 \cdot 10^{20} \text{ (N}\cdot\text{m/s}^2)$ by Satoh [10].

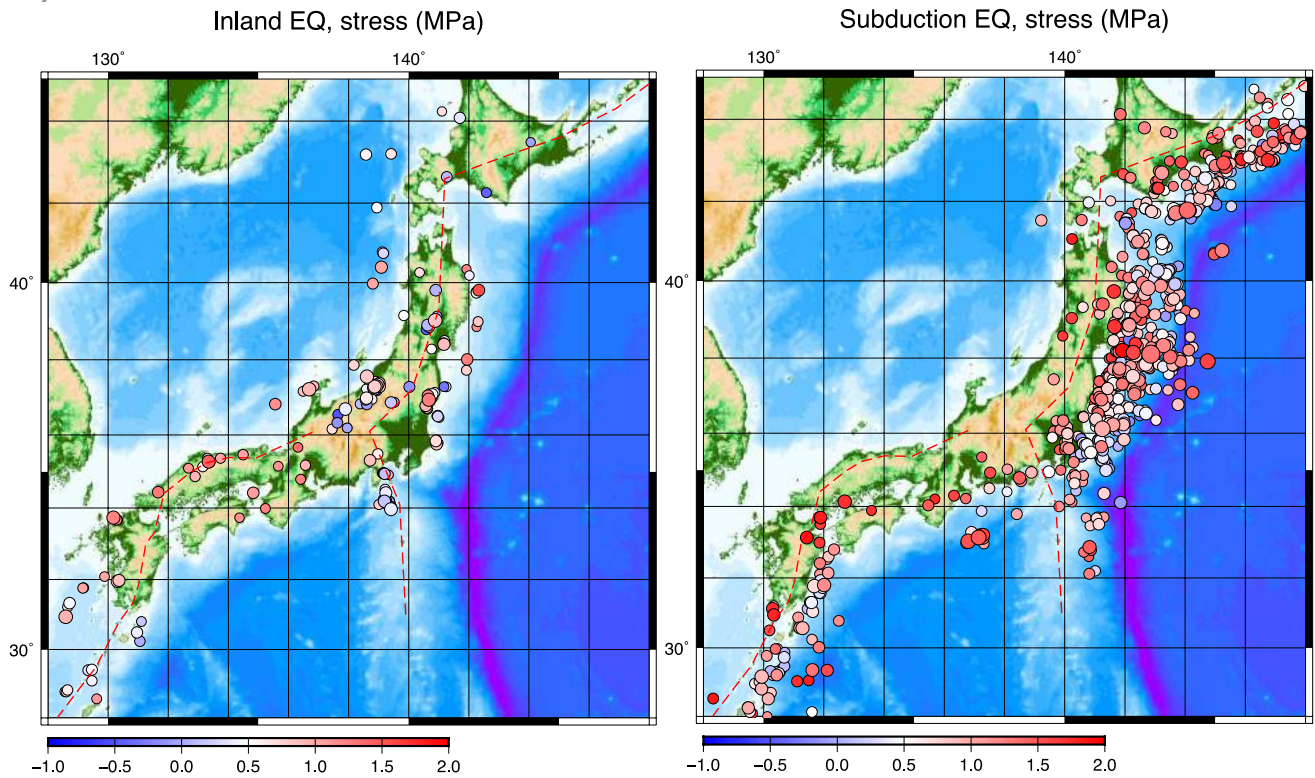


Fig.3 – Distribution of estimated stress drops. Scale bars indicate log (MPa)

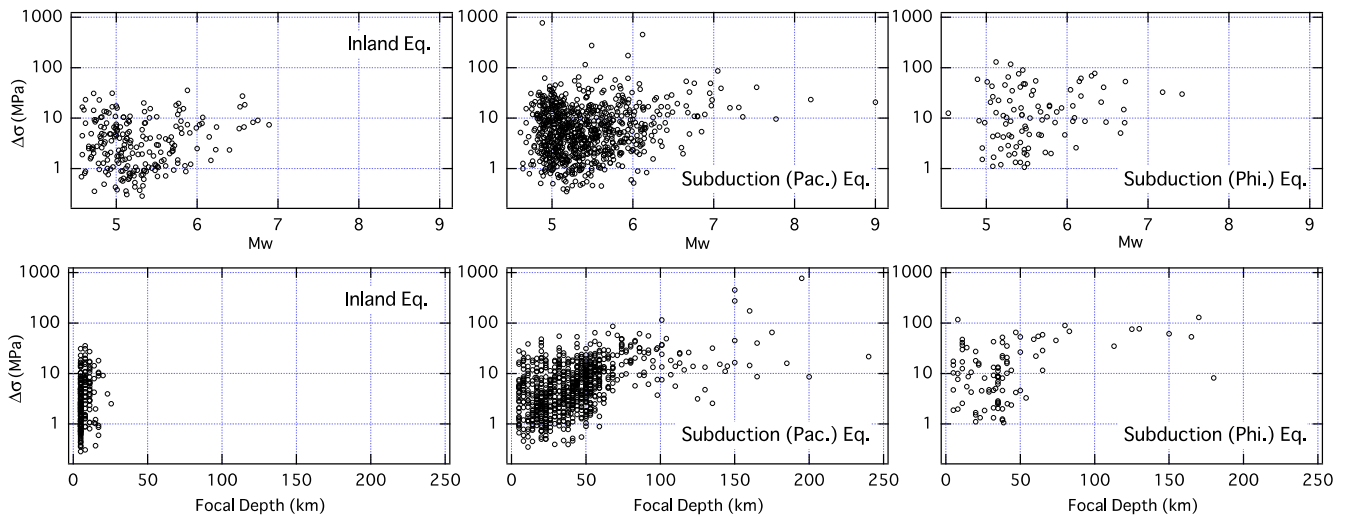


Fig. 4 – Relationships between estimated stress drops and Mw, focal depths.

3.3 Site amplification factor and standard error

Fig. 5 shows a map of the p_{Sv} amplification factors at 0.2Hz with topography. It is clearly found that the site amplification factors are large in the major plains and basins. Fig. 6 shows standard errors obtained from the spectral inversion analyses. The variability of FS is systematically larger than that of p_{Sv}, although the reason is not obvious.

Site Amp. Factor (0.2Hz)

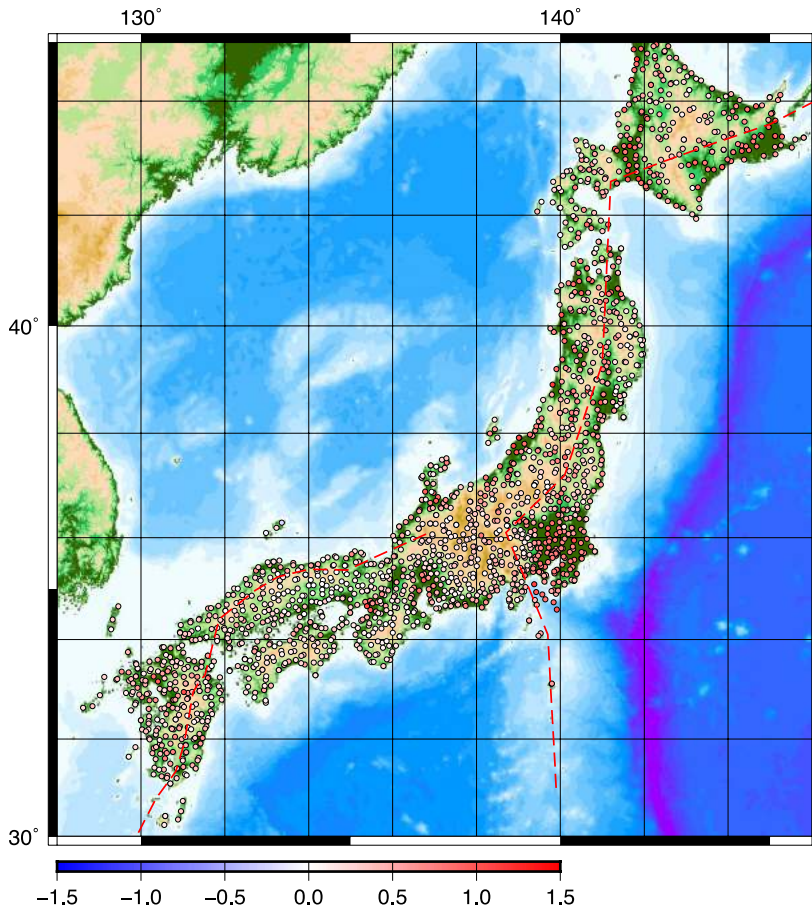


Fig. 5 – Distribution of estimated site amplification factors for pSv. Scale bar indicates log of amplification factor.

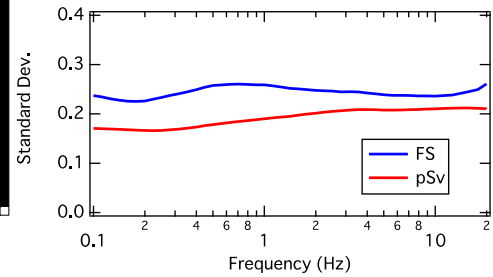


Fig. 6 – Standard deviations.

4. Modeling of site amplification factors and earthquake terms

To make GMPEs for FS, pSv, PGA, PGV, the estimated site amplification factor $G(f)$ is modeled as a function of V_{s30} and $D20$, and earthquake term $S(f)$ is modeled by M_w and $\Delta\sigma$.

4.1 Linear site amplification factor modeling

The estimated site amplification factors are modeled in Eqs. (11) and (12) as functions of V_{s30} and basin depth. V_{s30} is calculated from K-NET and KiK-net site profiles and the subsurface structure model for long period ground motion prediction map (Ver. 2012) [11] is used for basin depth. After several trials, $D20$ (upper depth of $V_{s2.0}$ km/s-layer) is adopted because the standard error become minimum than the other layers.

$$\log G_j(f) = c_1(f) \log(V_{s30_j}) + c_3(f) \quad (11)$$

$$\log G_j(f) = c'_1(f) \log(V_{s30_j}) + c'_2(f) \log(D20_j) + c'_3(f) \quad (12)$$

The estimated coefficients with the standard deviations are shown in Fig. 7. It is found that 1) the dependency on V_{s30} of pSv is stronger than that of FS, 2) the dependency on $D20$ in the lower frequency range is stronger than the high-frequency range, and 3) the variability of FS become large at high frequencies. The bottom right part of Fig. 7 is the relation between 0.2Hz-residuals to Eq. (11) and $D20$. As clear dependence on

D20 is found in D20>0.3km, Eq. (12) is better for that range. This is supported that the standard error of Eq. (12) becomes smaller in the low frequency range, compared with Eq. (11).

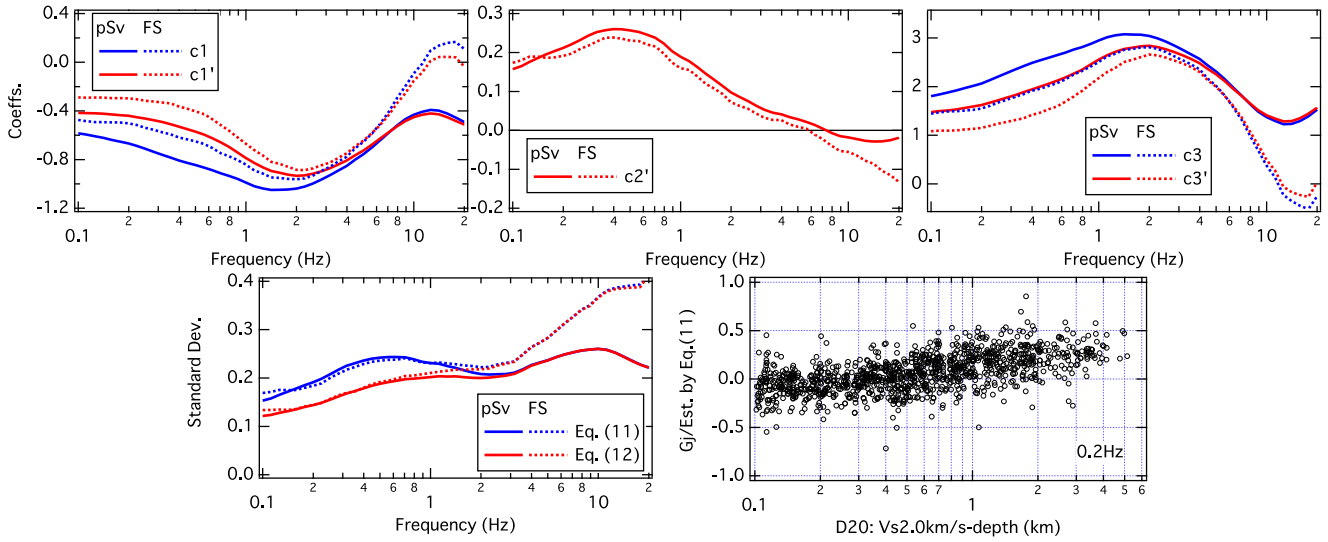


Fig. 7 – Regression coefficients for site amplification factors (top), standard deviations (bottom left), residuals by Eq. (11) (bottom right).

4.2 Earthquake term modeling

When earthquake term $S(f)$ follows omega-square model, the dependency of high-frequency level of $S(f)$ on M_w and $\Delta\sigma$ is expressed by Eq. (13). Based on this equation, $S(f)$ is modeled as Eq. (14). Quadratic equation is adopted to represent omega-square model in the wide magnitude range.

$$S_i(f) \propto M_o^{1/3} \Delta\sigma^{2/3} \propto 10^{0.5M_{wi}} \Delta\sigma^{2/3} \quad (13)$$

$$\log S_i(f) = a_1(f)M_{wi} + a_2(f)M_{wi}^2 + a_3(f)\log \Delta\sigma + a_4(f) \quad (14)$$

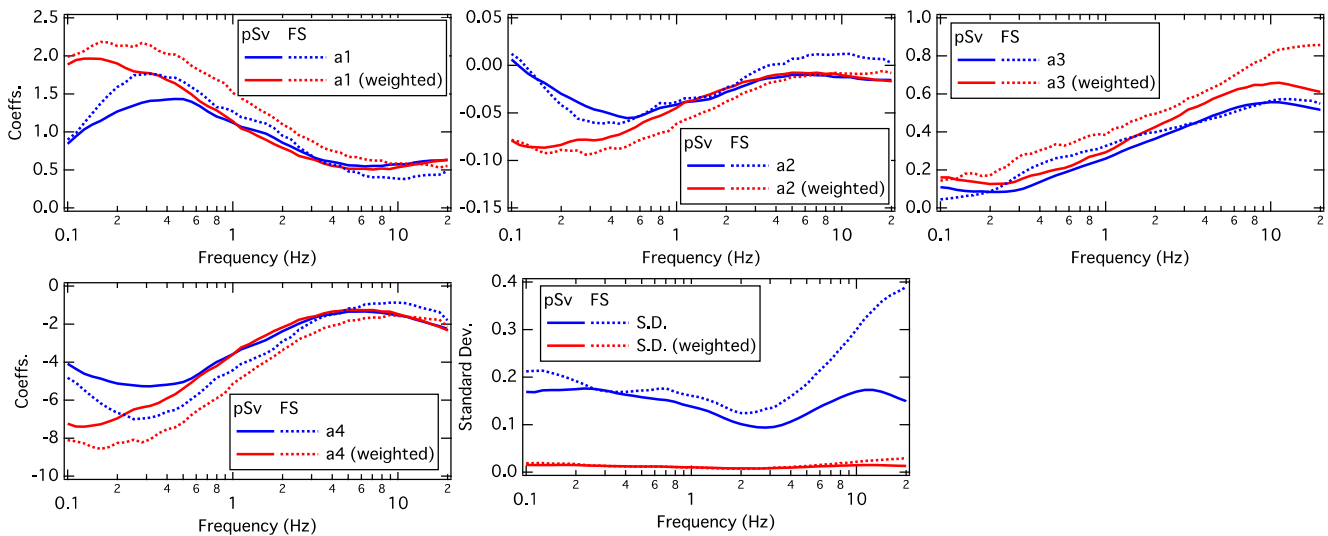


Fig. 8 – Regression coefficients for earthquake term.

After trying ordinary least squares method, it is found that the modeled long-period amplitude tends to overestimate for Mega earthquakes because distribution of the earthquakes concentrates in the small magnitude range as shown in Fig. 1. Thus, weighted regression analysis is applied by using the number of earthquakes in 0.5 magnitude intervals as weight. The estimated coefficients with the standard deviations are shown in Fig.8. The difference by weighting appears only in the low frequency range (less than 0.5Hz), but both of the linear (a_1) and quadratic (a_2) terms have larger coefficients compared with the ordinary regression. It is also found that the coefficients of FS are systematically larger compared with pSv, probably due to the effect of duration. Stress drop coefficient a_3 has larger values as frequencies become higher.

5. GMPE application and correction factor for nonlinear soil amplification

5.1 Application of the GMPE estimated in this study

Based on the results described above, the GMPE of this paper is constructed by combining Eqs. (3) to (5) with Eq. (11) or (12) and Eq. (14). Table 1 shows the coefficients for PGA and PGV. Fig. 9 shows the application examples for M7, M8, M9-class subduction earthquakes, and it is found that the developed GMPE can evaluate pSv in wide magnitude range. In Fig. 9, the estimates by O2008 [2], which is adopting linear Mw term, are also plotted. This figure shows that the linear Mw term tend to overestimate for Mega earthquake in low frequency range, but the quadratic equations used in this study can evaluate pSv even for M9-class Mega earthquakes.

Table 1 – Coefficients for PGA and PGV

Item	b_IL*	b1_pac*	b2_pac*	b1_phi*	b2_phi*	a1	a2	a3	a4
PGA	-0.00560	-0.00285	-0.00562	-0.00380	-0.00560	0.632	-0.015	0.560	-0.427
PGV	-0.00382	-0.00209	-0.00341	-0.00257	-0.00391	1.032	-0.035	0.365	-3.345
Item	c1	c3	c1'	c2'	c3'	d1	d2		
PGA	-0.639	1.969	-0.630	0.009	1.951	-0.697	1.767		
PGV	-0.853	2.579	-0.740	0.106	2.357	-0.494	0.641		

* b is coefficient of X_{eq} and related to Q as $Q = -\log e \times \rho \times b / V_s$ in Eq.(3) ($f=1\text{Hz}$)

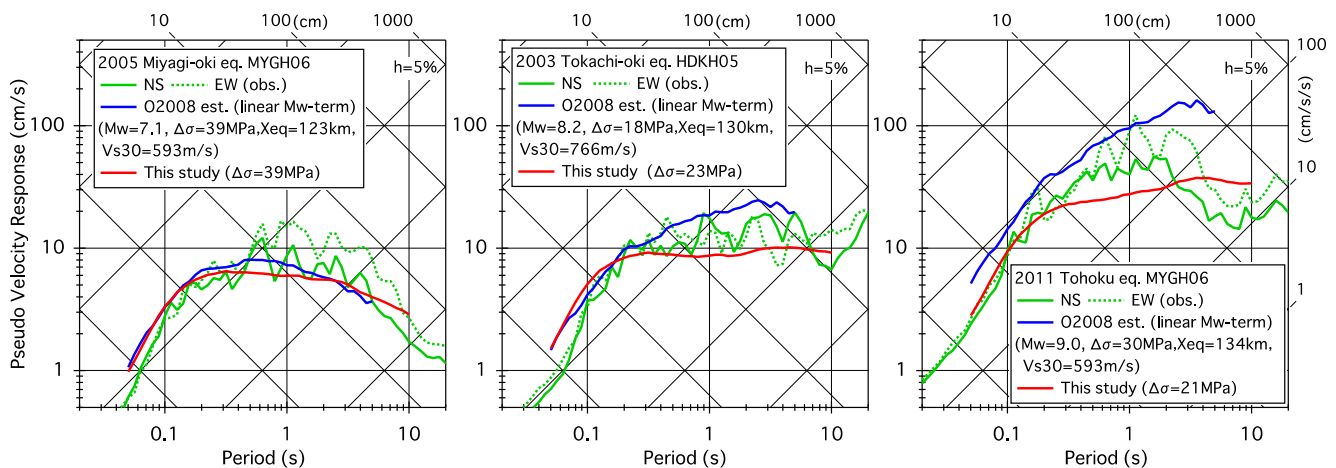


Fig. 9 – Application example for M7, M8, M9 earthquakes

Figure 10 shows PGV estimates of the developed GMPE with the observations of the 2011 Tohoku earthquake (M9.0) for three geological site classifications: rock, Pleistocene, and Holocene. Note that the estimates are multiplied by 1.4 because the observed PGVs are the larger horizontal components but the estimates correspond to the geometrical means. The estimates by Si and Midorikawa [12] (SI1999 in the figure), which is also derived using the Japanese strong-motion data with $5.8 \leq M_w \leq 8.2$, are also plotted. Both of the estimates are within the observed PGV distributions, while it is found that the estimates in this paper are closer to center of the observed distributions.

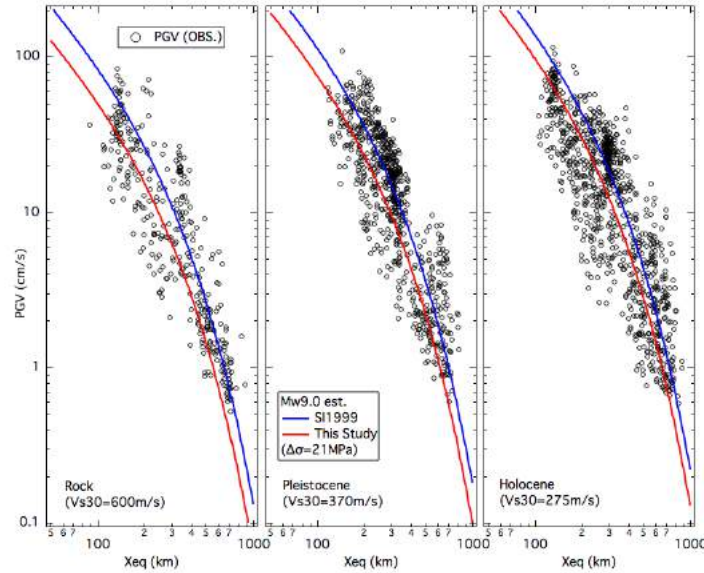


Fig. 10 – Application of the developed GMPE and the Si and Midorikawa's relation [12] to the 2011 Tohoku earthquake (Mw9.0).

5.2 Correction factor for nonlinear soil amplification

As described before, the regression analysis is conducted for $PGA < 200 \text{ cm/s}^2$ data. To check the applicability to large amplitude records, the ratios between large PGA data (over 200 cm/s^2) and the linear estimates at the ground surface by using Eq. (3) to (5) are calculated. The left part of Fig.11 shows the results. Red marks indicate large PGA data, showing that the ratio is smaller as the estimates become larger. This seems the effect of nonlinear soil response.

The correction factor of the nonlinear amplifications is modeled as Eq. (15), where $O(f)$ is observed pSv and $E(f)$ is estimated pSv. The estimated coefficients with standard deviations are shown in the middle and right parts of Fig. 11. Clear dependence on the linear estimates is observed especially in the high-frequency range. The author also tried to incorporate V_{s30} to the correction factor, but the standard deviation did not decrease. This needs further investigation.

$$\log[O(f)/E(f)] = d_1(f) \log E(f) + d_2(f) \quad (15)$$

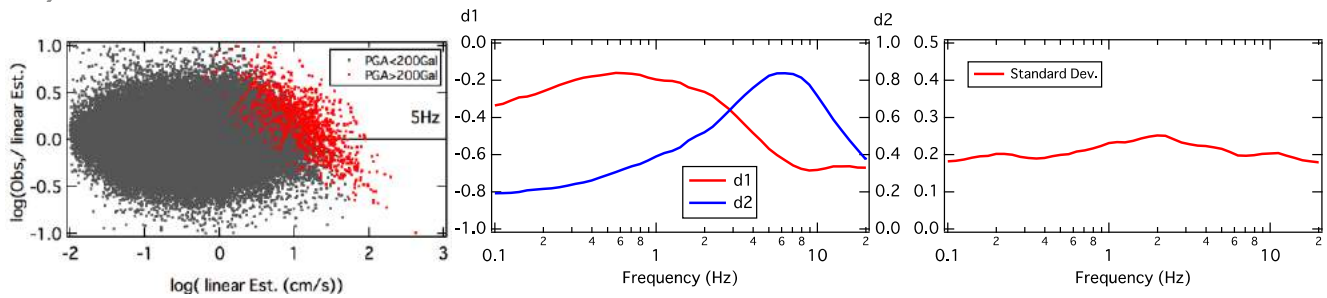


Fig. 11 – Correction coefficients for nonlinear site amplification. Relation between residuals and linear estimation at GL (left), Regression coefficients (middle), standard deviation (right)

6. Conclusions

A ground motion prediction equation for strong motion spectra is empirically developed using the 1996-2015 K-NET and KiK-net database in Japan. The M_w and distance range from 4.5 to 9.0 and less than 300km, respectively. The GMPE parameters are M_w , stress drop, X_{eq} , region of Q , V_{s30} and basin depth. As X_{eq} can incorporate the effects of fault extension and inhomogeneous energy radiation, and stress drops with M_w can incorporate short-period acceleration level into GMPE, the developed GMPE is applicable even for the case of several SMGAs of mega earthquake. Site amplification factors are also modeled by V_{s30} and basin depth. Nonlinear site amplification correction factor is also investigated.

7. Acknowledgements

NIED K-NET and KiK-net strong motion records are used. This research was supported by JSPS KAKENHI Grant Number 26420542. Fig. 3 and Fig. 5 are drawn by the GMT software [13].

8. References

- [1] Ohno S, Ohta T, Ikeura T, Takemura M (1993): Revision of attenuation formula considering the effect of fault size to evaluate strong motion spectra in near field, *Tectonophysics*, **218**, 69-81.
- [2] Ohno S (2008): Development of a statistical strong-motion evaluation method considering regional variation of source and path effects in the Tohoku region, Japan, *14th World Conf. Earthq. Eng.*, 02-0072.
- [3] Takai N, Okada S. (2002): Improvement of Attenuation Formula of Earthquake Ground Motion in Consideration of the Volcanic Front, *Proc. of the 11th Japan Earthquake Engineering Symposium*, 605-608.
- [4] Morikawa N, Fujiwara H (2013): A New Ground Motion Prediction Equation for Japan Applicable up to M9 Mega-Earthquake, *Journal of Disaster Research*, **8**, 878-888.
- [5] Sato R (1989): Handbook of fault parameters for Japanese earthquakes, Kajima Institute Publishing Co. LTD.
- [6] Satoh T, Tatsumi Y (2002): Source, Path, and Site Effects for Crustal and Subduction Earthquakes Inferred from Strong Motion Records in Japan, *J. Struct. Constr. Eng.*, **556**, 15-24. (in Japanese with English abstract)
- [7] JNES (2004): <https://www.nsr.go.jp/archive/jnes/atom-pdf/seika/000005449.pdf>
- [8] Satoh T (2016): Causes of Large Ground Motions at K-NET Tsukidate and KiK-net Haga during the Tohoku Earthquake based on the Analysis of Weak and Strong Motion Records, *Journal of Japan Association for Earthquake Engineering*, **16**, 4_52-4_65.
- [9] Asano K. and Iwata T (2012): Source model for strong ground motion generation in 0.1-10 Hz during the 2011 Tohoku earthquake, Special Issue: The 2011 Tohoku Earthquake. *Earth Planets Space*, **64**, 111-1123.
- [10] Satoh T. (2012): Inversion of source model of the 2011 off the Pacific coast of Tohoku earthquake using empirical Green's function method, *15th World Conf. Earthq. Eng.*, 0974.



- [11] The Headquarters for Earthquake Research Promotion (2012): http://www.jishin.go.jp/evaluation/seismic_hazard_map/lpshm/12_choshuki/
- [12] Si H, Midorikawa S (1999) New attenuation relationships for peak ground acceleration and velocity considering effects of fault type and site condition. *J. Struct. Constr. Eng*, **523**, 63-70. (in Japanese with English abstract)
- [13] Wessel P, Smith W. H. F. (1991): Free software helps map and display data, *EOS Trans. AGU*, **72**, 441.